Cascades in Wall-Bounded Turbulence

Javier Jiménez

School of Aeronautics, Universidad Politécnica, 28040 Madrid, Spain, and Center for Turbulence Research, Stanford University, Stanford, California 94305;
email: jimenez@torroja.dmt.upm.es

Annu. Rev. Fluid Mech. 2012. 44:27–45

First published online as a Review in Advance on September 1, 2011

The *Annual Review of Fluid Mechanics* is online at fluid.annualreviews.org

This article's doi:
10.1146/annurev-fluid-120710-101039

0066-4189/12/0115-0027$20.00

Keywords

boundary layers, cascade, simulation, logarithmic layer

Abstract

The kinematics and dynamics of wall-bounded turbulence are surveyed, with emphasis on the multiscale processes associated with the logarithmic layer and with its interactions with the wall. It is shown that the logarithmic law reflects a momentum cascade and that its structure agrees reasonably well with Townsend's (1961) model of a self-similar family of attached eddies, each of which contains, on average, a sweep-ejection pair, a segment of a large velocity streak, and disorganized vorticity. Those logarithmic eddies are themselves turbulent objects and can be studied in minimal simulation boxes that are much larger than those in the buffer layer. It is argued that, near the wall, the logarithmic eddies are probably the same as the vortex packets identified by experiments, but that their dynamics does not appear to be especially linked to the buffer layer. Further from the wall, they align into longer superstreaks, although the mechanism remains unclear.

1. INTRODUCTION

Wall-bounded turbulent flows are of huge technological importance. Roughly half the energy spent in transporting fluids through pipes and canals, or vehicles through air and water, is dissipated by turbulence in the immediate vicinity of walls. In this review, we concentrate on cases with little or no longitudinal pressure gradients, such as pipes, channels, and attached boundary layers. It was in such flows that turbulence was first studied scientifically (Darcy 1854, Hagen 1839), but they remain to this day less understood than homogeneous or free-shear flows. Turbulence is a multiscale phenomenon. Energy resides in the largest eddies and cannot be dissipated until it is transferred to the smaller ones, in which viscosity acts. The classical conceptual framework for that process is the self-similar Richardson (1920) cascade, which assumes that the transfer is local in scale, with no significant interactions between eddies of very different sizes. From energy-conservation arguments, Kolmogorov (1941) derived how energy is distributed among the eddies of the inertial range of isotropic flows and estimated the viscous length scale at which energy is finally dissipated, $\eta = (\nu^3/\epsilon)^{1/4}$, where ϵ is the rate of energy transfer and ν is the kinematic viscosity. It is interesting that the theory for the logarithmic velocity profile (which, as shown below, can be interpreted as a cascade of momentum in wall-bounded flows) was formulated by Millikan (1938) even before the Kolmogorov theory for the energy, although its mechanistic eddy model had to wait until Townsend (1961).

Isotropic theory gives no indication of how energy is fed into turbulence. The mechanism in shear flows is the interaction of the mean velocity gradient with the momentum flux carried by the velocity fluctuations. Turbulence, and especially scale change, is nonlinear, but the energy-injection process often can be described linearly because the timescale of the mean shear is faster than the turnover time of the largest eddies. In free-shear flows, such as jets and mixing layers, that mechanism leads to large-scale instabilities of the mean velocity profile (Brown & Roshko 1974, Gaster et al. 1985) and to energy-containing eddies of the order of the flow thickness. Most wall-bounded flows are not unstable in the same way (Reynolds & Tiederman 1967), but their largest scales are still probably linear. One of the most intriguing discoveries of the 1990s was that even stable perturbations can grow substantially by extracting energy from the mean flow (Schmid 2007) and that it is possible to relate such transient growth to some of the structures of wall-bounded turbulence (Butler & Farrell 1993, del Álamo & Jiménez 2006). However, many details of that relationship remain poorly understood.

The most interesting aspect of shear flows is not so much how energy is transferred across scales, but the spatial energy- and momentum-redistribution mechanisms. Wall-bounded flows are also inhomogeneous and anisotropic, and the wall segregates them into layers that have to be studied separately. Even so, our knowledge of wall turbulence has increased substantially over the past few years, partly because of new experimental techniques, but especially from the direct numerical simulations that followed the seminal work of Kim et al. (1987). Reviews of those early years are Robinson (1991), Panton (2001), and the papers collected in McKeon (2007), most of which center on the viscous layers closest to the wall, which were the only ones accessible at the relatively low Reynolds numbers initially available. Because of space limitations, we do not dwell on that fascinating topic and center our discussion on the multiscale mechanisms of the outer layers and on their interactions with the near-wall region. Both are beginning to emerge as the Reynolds numbers of experiments and simulations increase. A recent review of the very high–Reynolds number limit is provided by Smits et al. (2011), who dealt mostly with statistical information. We concentrate on structural aspects that have, at the moment, been studied only at more moderate Reynolds numbers, particularly on those suggested by numerical simulations. A survey of the models developed from experimental observations is provided by Adrian (2007).

A relatively recent development is the widespread availability of electronic data, some in raw form, which can be used by researchers outside the originating groups to develop and validate theories. A useful collection of relatively classical statistical turbulence data is AGARD (1998), and a website hosting this database also contains raw simulations of turbulent boundary layers and channels (**http://torroja.dmt.upm.es/ftp**). Many of the web pages of the groups cited below include similar collections.

In addition, we mention a subject that is closely related to this review. It is common experience that turbulence contains coherent structures with long lifetimes, ranging from the above-cited large-scale eddies of jets and shear layers to the sublayer streaks first identified by Kline et al. (1967) in wall-bounded flows. Their prevalence raises the question of whether they can be identified with underlying equilibrium, or otherwise simple, solutions of the equations of motion, which are almost certainly unstable and experimentally unobservable but may influence statistics and be extracted numerically. A review by Kawahara et al. (2012) can be found elsewhere in this volume.

The organization of the article is as follows. The following section summarizes the classical theory of wall-bounded turbulence, followed in Section 3 by a short review of the existing and prospective numerical simulations. The statistical evidence on the interaction among different layers is treated in Section 4, followed in Section 5 by a survey of the available structural models, and by discussion.

2. THE CLASSICAL THEORY

The spectral distributions of energy and dissipation in a typical wall-bounded flow are shown in **Figure 1*a***, in which each horizontal section is a spectral density at a given wall distance, plotted in terms of the streamwise wavelength. As in all turbulent flows, the energy is at the largest scales, whereas the dissipative eddies, represented by the vorticity magnitude, are smaller. However,

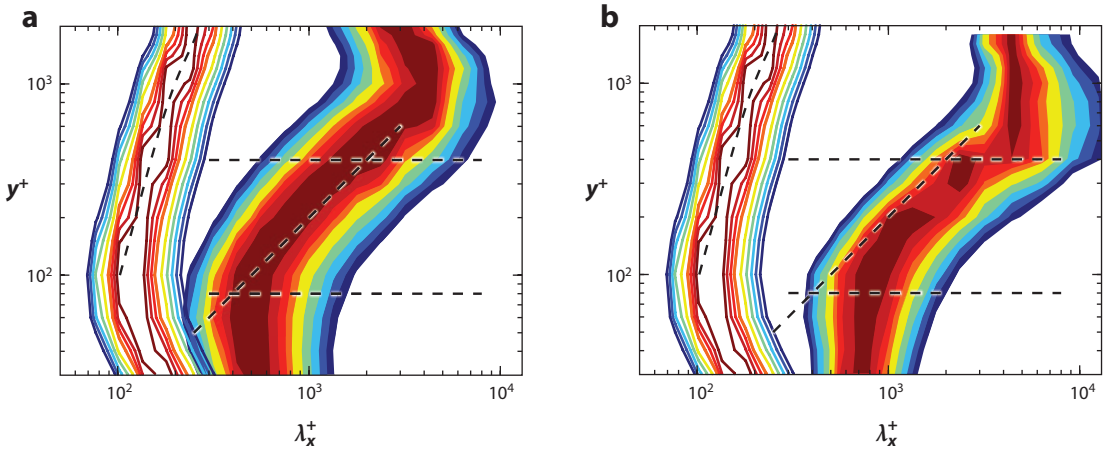

Figure 1

Spectral densities in a numerical turbulent channel at $\delta^+ = 2{,}000$, as functions of the streamwise wavelength λ_x and of the wall distance y. The shaded contours in panel *a* are the kinetic energy of the velocity fluctuations, $k_x E_{\mathbf{uu}}(k_x)$, and those in panel *b* are cospectra of the tangential Reynolds stress, $-k_x E_{\mathbf{uv}}(k_x)$. In both panels, the line contours are spectra of the surrogate dissipation, $\nu k_x E_{\omega\omega}(k_x)$, where ω is the vorticity magnitude. At each y, the lowest contour is 0.86 times the local maximum. The horizontal lines, $y^+ = 80$ and $y/\delta = 0.2$, are the approximate limits in which the energy length scale grows linearly with y. The diagonal lines through the two shaded spectra are $\lambda_x = 5y$. Those through the dissipation spectra are $\lambda_x = 40\eta$.

THE TURBULENT CASCADE

The classical model for the turbulent cascade is that energy, momentum, and other conserved quantities are transferred across the scale hierarchy when eddies either break or merge into smaller or larger ones. Whether the cascade is toward smaller (direct) or larger (inverse) sizes depends on the type of flow and on the transferred quantity. There is widespread agreement that the energy cascade in homogeneous flows is, on average, from the largest energy-containing eddies to the viscous Kolmogorov sizes and that it happens incrementally across an inertial range in which neither viscosity nor the character of the largest scales matters. The evidence is that the same is true in wall-bounded flows at a constant distance from the wall. The energy-containing eddies in **Figure 1*a*** dissipate mostly by inertial fragmentation without traveling substantially with respect to the wall, although there are other flows of energy and momentum moving away or toward the wall. However, as seen in the figure, the range of sizes spanned by the cascade depends on y, and whether an eddy can be considered large, viscous, or inertial depends on how far from the wall it is located.

because the flow is inhomogeneous, the size of the energy-containing eddies changes with the distance to the wall. Except for small imbalances very near and very far from the wall, most of the turbulent kinetic energy is dissipated at the same wall distance at which it is produced (Hoyas & Jiménez 2008), essentially as in the Kolmogorov cascade, but **Figure 1*a*** shows that the eddies containing most of the energy at one wall distance would be in the midst of the inertial cascade if they were moved further away (see the sidebar The Turbulent Cascade). The Reynolds number, defined as the scale disparity over which energy has to cascade toward dissipation, also changes with the wall distance.

We denote the boundary-layer thickness by δ, which also stands for the half-width and radius of the channels and pipes. Variables scaled with ν and with the friction velocity $u_\tau = \tau_w^{1/2}$, defined in terms of the wall shear stress τ_w, are said to be in wall units and are denoted by a plus superscript. Because we restrict ourselves to incompressible flows, the fluid density is set to one and dropped from the equations. Capitals are used for instantaneous values, lowercase symbols for fluctuations with respect to the mean, and primes for the root-mean-squared fluctuation intensities. The average $\langle\cdot\rangle$ is defined over many equivalent independent experiments, unless otherwise noted. The streamwise, wall-normal, and spanwise coordinates and velocity components are x, y, and z and U, V, and W, respectively.

Wall-bounded turbulence over smooth walls is described by two sets of scaling parameters (Tennekes & Lumley 1972). Viscosity is important near the wall, where lengths and velocities scale in wall units. **Figure 1** shows that the smallest structures in that region have sizes of the order of $100\nu/u_\tau$, with no scale disparity between energy and dissipation. The distance y^+ is a Reynolds number for the structures reaching from y to the wall and is never large within this layer, which is typically defined as $y^+ \lesssim 150$ (Österlund et al. 2000). It is conventionally divided into a viscous sublayer, $y^+ \lesssim 10$, in which viscosity is dominant, and a buffer layer, in which both viscosity and inertial effects have to be taken into account.

Away from the wall, the velocities also scale with the friction velocity because momentum conservation requires that the tangential Reynolds stress, $-\langle uv\rangle$, only changes slowly with y to compensate for the pressure gradient. The length scale far from the wall is the flow thickness δ, and the ratio between the largest and smallest scales in **Figure 1*a*** is approximately $\delta^+/100$, where $\delta^+ = u_\tau\delta/\nu$ is the friction Reynolds number.

Models for wall-bounded turbulence have to deal with spatial fluxes that are absent from the homogeneous case. The most important one is that of momentum. Let us consider a turbulent

channel between infinite parallel planes. Momentum is fed over the whole cross section by the pressure gradient and carried by the Reynolds stress to be removed by friction at the wall. **Figure 1*b*** shows that the stress resides in eddies of roughly the same size as the energy and that, as momentum is transferred along y, it has to change size by about the same amount as the energy across its cascade. Momentum transport is present in all shear flows, but its multiscale character is restricted to very inhomogeneous situations, such as the present one.

The transition between the inner and outer length scales occurs in an intermediate logarithmic layer, in which the only available scale is the distance y to the wall. In **Figure 1**, this is the range $y^+ \gtrsim 80$, $y/\delta \lesssim 0.2$, where the size of the energy-containing eddies is proportional to y. We see below that large-scale eddies of size $O(\delta)$ penetrate all the way to the wall and that the velocity does not scale strictly with u_τ. Both the constant velocity scale and the absence of a length scale other than y are only approximations, but if they are accepted, Townsend (1976) showed that the mean velocity should be

$$\langle U \rangle^+ = \kappa^{-1} \log y^+ + A. \tag{1}$$

This form agrees well with experimental evidence, with an approximately universal Kármán constant, $\kappa \approx 0.4$, and an intercept A that depends on the details of the near-wall region. For smooth walls, $A \approx 5$.

The viscous, buffer, and logarithmic layers constitute the main difference between wall-bounded flows and other turbulence. Even if they are geometrically thin with respect to the flow as a whole, they are extremely important. The friction Reynolds number ranges from $\delta^+ = 200$ for barely turbulent flows to 10^6 for large water pipes. In the latter, the near-wall layer is only approximately $150/\delta^+ \approx 10^{-4}$ times the pipe radius, but it follows from Equation 1 that, even in that case, 40% of the velocity drop, and of the energy dissipation, takes place below $y^+ = 80$.

Most of the velocity difference that does not reside in the near-wall viscous region is concentrated in the logarithmic layer. The velocity difference above $y = 0.2\delta$ is approximately 20% of the total when $\delta^+ = 200$ and decreases logarithmically as the Reynolds number increases. In the limit of very large Reynolds numbers, all the velocity drop is in the logarithmic layer.

The logarithmic layer is an intrinsically high–Reynolds number phenomenon. Its existence requires, at least, that its upper limit should be above the lower one so that $0.2\delta^+ \gtrsim 150$, and $\delta^+ \gtrsim 750$. The requirements become stricter if a substantial logarithmic range is desired.

3. NUMERICAL SIMULATIONS

The logarithmic layer has been studied experimentally for a long time, but numerical simulations with even incipient logarithmic regions have only recently become available. The channel simulations of Kim et al. (1987) had $\delta^+ = 180$, and therefore essentially no scale range, but the Reynolds numbers of numerical flows have increased steadily, and the channels by Abe et al. (2004), del Álamo et al. (2004), and Hoyas & Jiménez (2006), or the boundary layers by Lee & Sung (2007, 2011), Schlatter et al. (2009), Simens et al. (2009), Wu & Moin (2010), and Sillero et al. (2010), with $\delta^+ \approx 1{,}000$–$2{,}000$, are comparable to most well-resolved experiments and have approximately a decade of scale disparity. For example, the range in which the wavelength of the spectral energy peak grows linearly with y in **Figure 1** spans a factor of five, from $y^+ = 80$ to $y^+ = 400$. Those simulations, as well as simultaneous advances in experimental observations, have greatly improved our knowledge of the kinematics of the outer-layer structures and are beginning to give some indications about their dynamics. Moreover, because the Reynolds numbers of simulations and experiments are beginning to be comparable, it is becoming possible to validate the structural

models suggested by experiments against time-resolved three-dimensional simulated flow fields (e.g., Lozano-Durán & Jiménez 2010), and vice versa.

It is important to realize that the process of increasing the Reynolds number of the simulations need not be open-ended. The goal of turbulence theory is not to reach ever-increasing Reynolds numbers, but to describe the flow well enough to make useful predictions. If we admit that the key complication of turbulence is its multiscale character, it is probably true that a fully resolved database of the space-time evolution of enough flows with a reasonably wide range of scales would contain all the information required to formulate a theory of turbulence. Of course, such a data set would not be a theory, but it is doubtful whether further increasing its Reynolds number would provide much additional help in formulating one. It is difficult to say a priori when that stage will be reached, but it is probably true that a further factor of 5–10 in δ^+ over that in **Figure 1**, which would give us a range of scales close to 50–100, would provide all the information required to understand most of the dynamical aspects of wall-bounded turbulence. With the usual estimate of the order of δ^{+3} for the cost of simulations, and the present rate of increase in computer speed of 10^3 per decade, it should be possible to compile such a database within the next decade.

4. INNER-OUTER INTERACTIONS

Figure 1 shows the representative scales of the different turbulent quantities but leaves out some important features. The first one is the presence of very large scales. The longest wavelengths in the figure are approximately 6δ ($\lambda_x^+ \approx 12{,}000$ at the Reynolds number of the figure), but structures two or three times longer are found experimentally in the outer layers of turbulent wall flows (Jiménez 1998, Kim & Adrian 1999). They are also relatively wide, $\lambda_z \approx 1$–2δ, and correlated across the whole flow thickness (del Álamo & Jiménez 2003, del Álamo et al. 2004). **Figure 2*a*** presents spectral densities of the kinetic energy in the buffer layer, and a comparison between

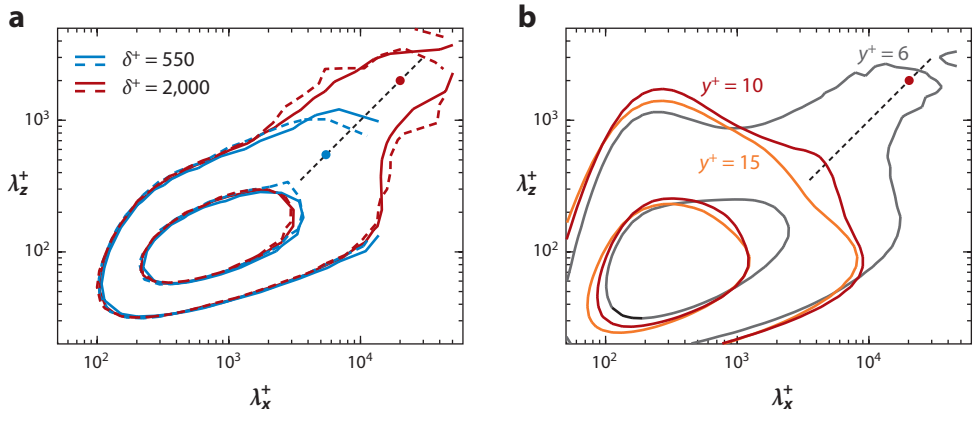

Figure 2

(*a*) Spectral densities of the kinetic energy, $k_x k_z E_{\mathbf{uu}}$, scaled in wall units, in the buffer region ($y^+ = 15$) of channels (*solid lines*) and boundary layers (*dashed lines*) at $\delta^+ = 550$ (*blue*) and 2,000 (*red*). The dashed black diagonal line is $\lambda_x = 10\lambda_z$, and the dots are $\lambda_z = \delta$. Contours are 0.125 and 0.5 times the maximum of the spectrum of the $\delta^+ = 2{,}000$ channel. (*b*) Spectral densities of the vorticity magnitude, $k_x k_z E_{\omega\omega}$, near the wall for the channel at $\delta^+ = 2{,}000$: $y^+ = 6$ (*black*), 10 (*red*), and 15 (*orange*). The dashed diagonal line and dot are as in panel *a*. Contours contain 0.5 and 0.9 of the enstrophy of each spectrum. Figure adapted from Hoyas & Jiménez (2008).

Figure 1 and the spectral handles in the upper-right corner of **Figure 2*a*** reveals that eddies from the outer edge of the logarithmic layer reach the wall. Hoyas & Jiménez (2006) showed that the intermediate scales within the handle are the roots of eddies whose energy and Reynolds stresses peak within the logarithmic layer. **Figures 1** and **2*a***, taken together, show that the cores of those eddies are at $y \approx \lambda_x/5$, $\lambda_x \approx 10\lambda_z$, and $y \approx 2\lambda_z$, implying that the structures that reach from the wall to height y are not much longer than $5y$ in the logarithmic layer, or much wider than $y/2$. Longer or wider structures are also taller.

Those attached eddies had been posited by Townsend (1961, 1976), who observed that turbulent eddies centered at distance y from the wall behave differently depending on whether they reach the wall. Detached eddies, with wall-normal dimensions smaller than y, feel the wall only indirectly (e.g., through the shear of the mean profile) and behave more or less as in free-shear flows. They are roughly isotropic and form classical Kolmogorov (1941) energy cascades. On the general argument that the energy of turbulent eddies increases with size, the most-intense detached eddies should be those with sizes roughly equal to y and therefore coincide with the smallest attached ones. Larger eddies cannot contain wall-normal velocity or tangential Reynolds stress because the impermeability condition damps v, but other variables can get wider and longer than $O(y)$. The absence of Reynolds stresses implies that the roots of those larger wall-attached eddies are irrotational because the only forces acting on them are pressure gradients. That is confirmed by the vorticity spectrum at $y^+ = 15$ in **Figure 2*b***, which lacks the large-scale handle. The handle reappears very near the wall, as shown by the other two spectra in **Figure 2*b***. Irrotational flow cannot satisfy enough boundary conditions to accommodate a no-slip wall, which is enforced by thin rotational viscous layers below $y^+ \approx 8$.

The attached-eddy idea has been used extensively to model wall turbulence and is behind the elementary arguments for the logarithmic velocity profile. The idea is that the mean tangential Reynolds stress, which has to be $O(u_\tau^2)$ to satisfy the momentum equation, is dominated at each wall distance by essentially single-scale active eddies of $\lambda_x = O(y)$. In practice, Guala et al. (2006) and Balakumar & Adrian (2007) have shown that active eddies may be quite long, with a substantial fraction of the Reynolds stress in structures longer than 10δ, but Jiménez & Hoyas (2008) surveyed the available experimental evidence and confirmed that the $-\langle uv \rangle$ cospectrum scales well with the distance to the wall. It peaks around $\lambda_x = 10y$ and is essentially zero beyond $\lambda_x = 100y$.

Above it is mentioned that the logarithmic layer is the momentum equivalent to the inertial energy cascade, and the attached-eddy model makes that correspondence precise. What was missing from Millikan's (1938) derivation of the logarithmic profile was the equivalent of Obukhov's (1941) model for the Kolmogorov (1941) homogeneous spectrum, in which eddies transfer their energy to an approximately space-filling cascade of smaller ones. In Townsend's (1961) model, larger attached eddies transfer their momentum to smaller ones closer to the wall. In the limit $Re \to \infty$, the homogeneous cascade results in singular gradients distributed uniformly over the whole flow, whereas the logarithmic one results in an accumulation point of singularities at the wall. Turbulence is characterized by the expulsion of the velocity gradients toward the small scales, away from the large energy-containing eddies. In wall-bounded flows, that separation occurs not only in the scale space for the energy dissipation, but also in the shape of the mean velocity profile for the momentum transfer. The singularities are expelled both from the large scales to the small ones and from the center of the flow toward the logarithmic and viscous layers.

Townsend (1976) noted that the above arguments imply that the wall-parallel velocity fluctuations below and within the logarithmic layer cannot simply scale with u_τ because, besides the active eddies of size $\lambda_x = O(y)$, they include extra inactive ones with $\lambda_x \gg y$. The intensities of those eddies are also $O(u_\tau)$ because they are the roots of taller eddies, active at wall distances $y_\lambda = O(\lambda_x) \gg y$. The result is that the intensities of the wall-parallel velocity components, and

of the pressure, should behave as

$$u'^2 \sim u_\tau^2 \log(\delta/y), \tag{2}$$

where $\log(\delta/y)$ is the number of logarithmic bands separating the largest scales of $O(\delta)$ from those of $O(y)$. That idea has been developed into fairly detailed models by Perry et al. (1986), Perry & Li (1990), and Kunkel & Marusic (2006), and the logarithmic profiles for the fluctuations are well satisfied experimentally for those variables that are not subject to blocking by the wall, especially w' and p' (Jiménez & Hoyas 2008). The logarithmic profile for u' has been the subject of more debate, probably in part because it is the one measured most often, but also because the energy in the near-wall spectral region is comparatively large and interferes with that of the logarithmic structures. The issue has been discussed at length by Smits et al. (2011), who concluded that there is probably no deviation from the logarithmic prediction if the Reynolds number is high enough. Recent results by Hultmark et al. (2010) suggest that some of the proposed effects, such as the presence of a second peak of u' in the logarithmic layer, probably result from either wall roughness or poor instrumental resolution. In fact, there is relatively little evidence for failures of self-similarity in the behavior of turbulent fluctuations in the logarithmic layer. Some of the effects that had been claimed, such as the ones just discussed, or the presence of an extra spectral peak (Kunkel & Marusic 2006), can be traced to instrument limitations (del Álamo & Jiménez 2009). The spectral distribution of the velocities in the logarithmic region is complicated and very anisotropic, and one advantage of numerical simulations is the possibility of observing it in detail, often allowing the identification of trends and artifacts at much lower Reynolds numbers than when relying only on integrated intensities or mean profiles.

In the buffer layer, Equation 2 implies that $u'^2 \sim u_\tau^2 \log(\delta^+)$ and that the energy of the near-wall velocity fluctuations would be dominated at very high Reynolds numbers by the large-scale spectral handle in **Figure 2*a***. That is confirmed by laboratory experiments (deGraaff & Eaton 2000), simulations (Hoyas & Jiménez 2006), and atmospheric observations (Metzger & Klewicki 2001, Kunkel & Marusic 2006). The argument also implies that the logarithmic dependence of the buffer-layer intensities should not be so much with δ^+ as with the range of length scales present in the spectrum. **Figure 2*a*** includes channels and boundary layers, and although the aspect ratio λ_x/λ_z of the spectral handle is the same for both, the boundary layers are slightly shorter and narrower (Monty et al. 2009, Jiménez et al. 2010). It is interesting that Iwamoto et al. (2006) compared different flows and found that their near-wall intensities correlate better with the maximum width of the large scales than with δ^+.

The presence of energetic outer scales in the buffer layer raises the question of whether the character of the near-wall region would change at very high Reynolds numbers, but the evidence is scarce. Klewicki et al. (1995) observed near-wall streaks, essentially identical to those at moderate Reynolds numbers, in atmospheric flows in which almost half the kinetic energy is contained in the spectral handle (Metzger et al. 2001). Bertschy et al. (1983), in thin water sheets, and Jiménez & Pinelli (1999), in manipulated simulations, showed that the near-wall turbulence cycle can run independently of the outer flow, with similar characteristics to those of full channels. The structures in the spectral handle are much larger than those involved in the buffer-layer cycle, which have characteristic widths $\lambda_z^+ \approx 100$. Even at the comparatively moderate Reynolds numbers of **Figure 2*a***, they are more than an order of magnitude larger than those at the core of the near-wall spectrum, which is the region that does not change between the two Reynolds numbers in the figure. In essence, the near-wall cycle lives in local boundary layers defined by the larger scales (Jiménez 2009).

Marusic et al. (2010) noted that the large scales partially modulate the near-wall cycle. The near-wall fluctuations are stronger underneath high-velocity regions even when the inactive energy

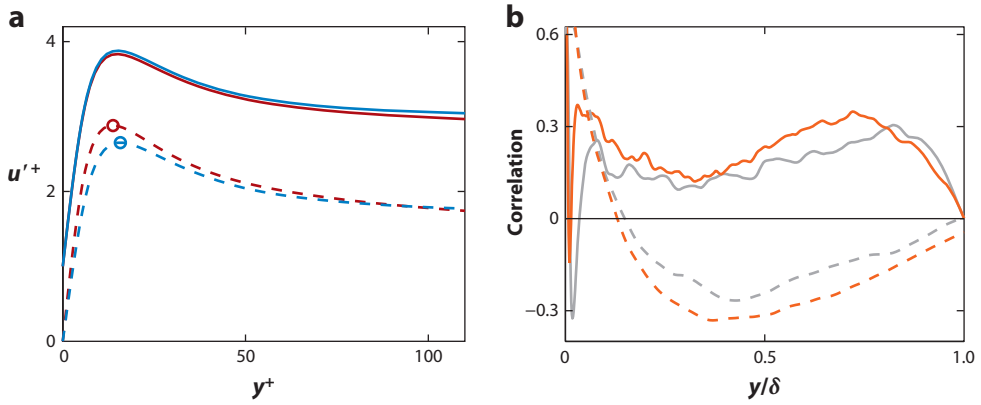

Figure 3

Fluctuation intensities computed over sub-boxes with dimensions $\lambda_x \times \lambda_z = 1.5\delta \times 0.75\delta$. (*a*) Streamwise fluctuations conditioned to boxes in which the friction velocity is more than one standard deviation above (*red*) or below (*blue*) average. For the dashed lines, the wall distance and velocities are normalized with the global friction velocity; for the solid ones, which are offset for clarity, they are normalized with the friction velocity local to each sub-box. The channel is at $\delta^+ = 2{,}000$ (Hoyas & Jiménez 2006). (*b*) Correlation coefficient of the wall-normal sub-box intensities with the sub-box friction velocity (*dashed lines*) and with the local sub-box velocity gradient (*solid lines*). The channels are at $\delta^+ = 934$ (*gray*) and 2,000 (*red*).

is subtracted, and the effect reverses in the outer part of the logarithmic layer (Mathis et al. 2009). The discussion in the previous paragraph suggests that the effect is a relatively local one in which the small-scale structures equilibrate with their large-scale environment. For example, **Figure 3*a*** shows intensity profiles computed over wall-parallel boxes of the order of δ^2. When they are normalized with the overall friction velocity, those in high-shear boxes are stronger and peak closer to the wall, but both effects disappear when the intensities and coordinates are normalized with the local friction velocity computed over each box. The same principle holds away from the wall. **Figure 3*b*** shows the correlation of the wall-normal intensities with the coarse-grained wall shear, which, as mentioned above, reverses sign around the middle of the logarithmic layer. The figure also shows that the correlation of the same quantity with the coarse-grained shear at the same height is uniformly positive, which is what would be expected if the fluctuations were in equilibrium with their local environment. The reason for the correlation reversal between the wall and the outside is that steep gradients at the wall correspond to shallow ones further away, and vice versa, essentially because the free-stream velocity is uniform.

The local-equilibrium idea is similar to the refined Kolmogorov (1962) hypothesis that small-scale fluctuations are in equilibrium with the local coarse-grained dissipation, rather than with the overall mean value, and suggests that intermittency effects could be expected near the wall, which would be different from those further away (see Benzi et al. 1999).

5. STRUCTURES

Structural models mean something different away from the wall than near it. Near the wall, the local Reynolds numbers are low, the flow is smooth, and one may speak of objects. Examples include the above-mentioned reviews by Panton (2001) and McKeon (2007) and papers by Jiménez & Moin (1991), Jiménez & Pinelli (1999), Schoppa & Hussain (2002), and Kawahara et al. (2012). Above the buffer layer, the internal Reynolds numbers of the eddies are $y^+ \gg 1$, implying that

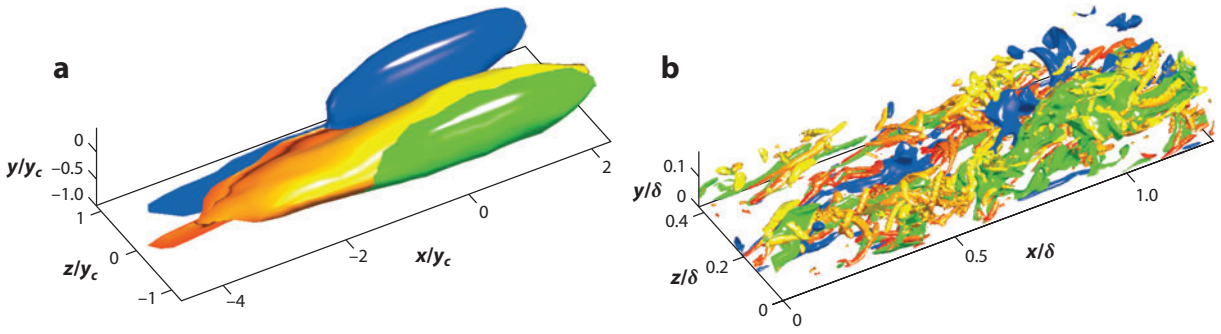

Figure 4

(*a*) Structure of the averaged Reynolds stress, conditioned to the presence of a sweep (*blue*), side by side with an ejection (*green*). The yellow object, redder toward the wall, is the mean location of the strong vorticity. The flow is from bottom left to top right, and the axes are scaled with the distance from the wall of the center of gravity of the Reynolds stress pair, which is oriented so that the sweep closest to the ejection is always to its left. The flow is a channel at $\delta^+ = 934$. (*b*) An instantaneous realization of the same object, with axes scaled with δ.

they are themselves turbulent, nonsmooth, and connected to the dissipative scales by cascades of length $y^{+3/4}$. An example of such a structure is shown in **Figure 4*b***. We can expect only statistical descriptions in that region, such as the conditional average in **Figure 4*a***, perhaps coupled with stochastic models for the cascade underneath.

The structural analysis of wall-bounded flows is not new. Sublayer streaks were first identified by Kline et al. (1967) and their dynamics qualitatively described by Kim et al. (1971). Next came quadrant analysis, in which each point of the u-v plane was classified into quadrants (Wallace et al. 1972, Willmarth & Lu 1972). Most of the average tangential stress originates either from the second quadrant (ejections, $u < 0$ and $v > 0$) or from the fourth (sweeps, $u > 0$ and $v < 0$). Intervals of strong Reynolds stress, defined by $-uv > H\,u'v'$, with H typically between 1 and 2, and the related VITA (variable interval time average) technique of Blackwelder & Kaplan (1976), were used to identify individual structures from single-point temporal signals. Buffer-layer ejections turned out to be spaced by approximately 500 wall units and were later associated with individual vortices (Robinson 1991), but they cluster into groups whose lengths, of the order of a few thousand wall units, suggest that they may be associated with events in the logarithmic layer (Bogard & Tiederman 1986). Visualizations and particle image velocimetry experiments in the 1990s provided two-dimensional flow sections and linked the groups of ejections to ramp-like, low-momentum regions surrounded by shear layers populated by intense transverse vortices. A popular interpretation has been that the ramps are packets of self-propelled hairpin vortices, each of which represents an individual ejection originating at the wall. Adrian (2007) gave a compelling exposition of that point of view.

However, it is unclear how far from the wall such an arrangement extends. A common criterion has been that vortices corotating with the shear, and therefore candidates for hairpin heads, should predominate over counterrotating ones. Wu & Christensen (2005) found that to be the case over the full logarithmic region below $y/\delta \approx 0.25$, but Carlier & Stanislas (2005) found both signs to be comparable above $y^+ \approx 150$ ($y/\delta \approx 0.06$), and Herpin (2010), over a wider range of Reynolds numbers, found that their ratio stabilizes above $y^+ \approx 400$. She also found that streamwise vortices dominate over transverse heads below $y^+ = 100$, in agreement with Robinson (1991). Working from x-z flow sections, Ganapathisubramani et al. (2003) identified organized vortex packets at $y^+ = 150$ ($y/\delta = 0.15$) but only disorganized ones above $y^+ = 200$, and Tomkins & Adrian (2003)

found long packets below $y^+ = 100$ but had to resort to statistical correlations to document the looser organization at $y^+ = 400$.

In fact, vorticity fluctuations above $y^+ \approx 100$ are isotropic, with the spectra of the three components centered around $\lambda = 40\eta$, as in **Figure 1**. Tanahashi et al. (2004) showed that the intense vortices in turbulent channels are identical to those in isotropic turbulence (Jiménez et al. 1993), and Saddoughi & Veeravali (1994) showed that the Reynolds stress tensor in a very high–Reynolds number boundary layer is essentially isotropic for wavelengths smaller than $\lambda \approx y/4$, including the dissipative range. That result agrees with Corrsin's (1958) criterion that eddies are isotropic when their internal gradients are larger than the ambient shear, $(\epsilon\lambda)^{1/3} \gtrsim \lambda\partial_y\langle U\rangle$, and implies that only structures of $O(y)$ need to be examined to understand momentum transfer.

When three-dimensional flow fields became available from simulations, it was possible to study directly the structure of the stresses in the logarithmic layer. Recognizing the ambiguities just discussed for individual vortices, del Álamo et al. (2006) considered large attached vortex clusters, which are shells of disorganized vorticity extending above $y^+ = 100$, whose thickness, $O(10\eta)$, is roughly the diameter of individual vortices. They mark ejections extending from the wall into the outer flow and form a self-similar family in $y^+ \gtrsim 50$, $y/\delta \lesssim 0.4$, with aspect ratios $L_x \times L_y \times L_z = 3 \times 1 \times 1.5$. Note that those ratios are shorter than the energy spectra in **Figures 1** and **2**. The dimensions of the clusters agree well with the spectrum $k_x k_z E_{vv}$ of the wall-normal velocity, which is shorter than $k_x k_z E_{uu}$ (**Figure 5*a***). When the flow is conditionally averaged around the clusters, it is found to contain a long, conical, low-velocity region whose intersection with a fixed y represents well the spectrum of u (del Álamo et al. 2006).

A more direct investigation of the momentum transfer was undertaken by Flores & Jiménez (2008), who studied the three-dimensional structures defined by the quadrant criterion discussed above. They found that sweeps and ejections are also self-similar above the buffer layer and tend to form side-by-side pairs, suggesting the flanks of a vortical structure in between. They also found that sweep-ejection pairs tend to be associated with vortex clusters, at least in the logarithmic region, forming a composite structure whose conditionally averaged organization is shown in **Figure 4*a***. The figure is a self-similar construct, compiled by averaging events of different sizes and heights, normalized with the distance to the wall of their centers of gravity. Its aspect ratio, $L_x \times L_y \times L_z = 4 \times 1 \times 1.5$, is comparable with that of the clusters. The conditionally averaged structure does not represent any individual realization, which tend to be asymmetric and disorganized. An example is given in **Figure 4*b***.

The instantaneous structures responsible for the long spectra of u are less understood. Clusters and ejections tend to align in streamwise groups, reminiscent of the hairpin packets mentioned above, but much longer (Flores & Jiménez 2008). Whereas the packets are at most $L_x \approx 3\delta$, the u spectra, or the conical wakes described by del Álamo et al. (2006), are between 5 and 10 times longer. They are probably the objects variously described as global modes by del Álamo & Jiménez (2003) and del Álamo et al. (2004), or as very-large-scale motions (VLSMs) or superstructures by Adrian (2007) and Smits et al. (2011), whereas the objects depicted in **Figure 4** are the large-scale motions (LSMs) of those authors. For example, the dimensions of the objects in **Figure 4** agree with the conditional structures isolated by Wark & Nagib (1991) using quadrant analysis. The global modes are not just statistical constructs. Very long cones are found in simulations (e.g., see Jiménez 2007, figure 5) and observed as low-momentum ramps in streamwise sections of instantaneous flow fields (Meinhart & Adrian 1995). They are relatively easy to isolate as connected regions with $u < -u'$ in the logarithmic layer. A typical example is the structure in **Figure 5*b***, which gives the impression of being formed by subunits of the size of the clusters or LSMs mentioned above. The meandering aspect of VLSMs was emphasized by Hutchins &

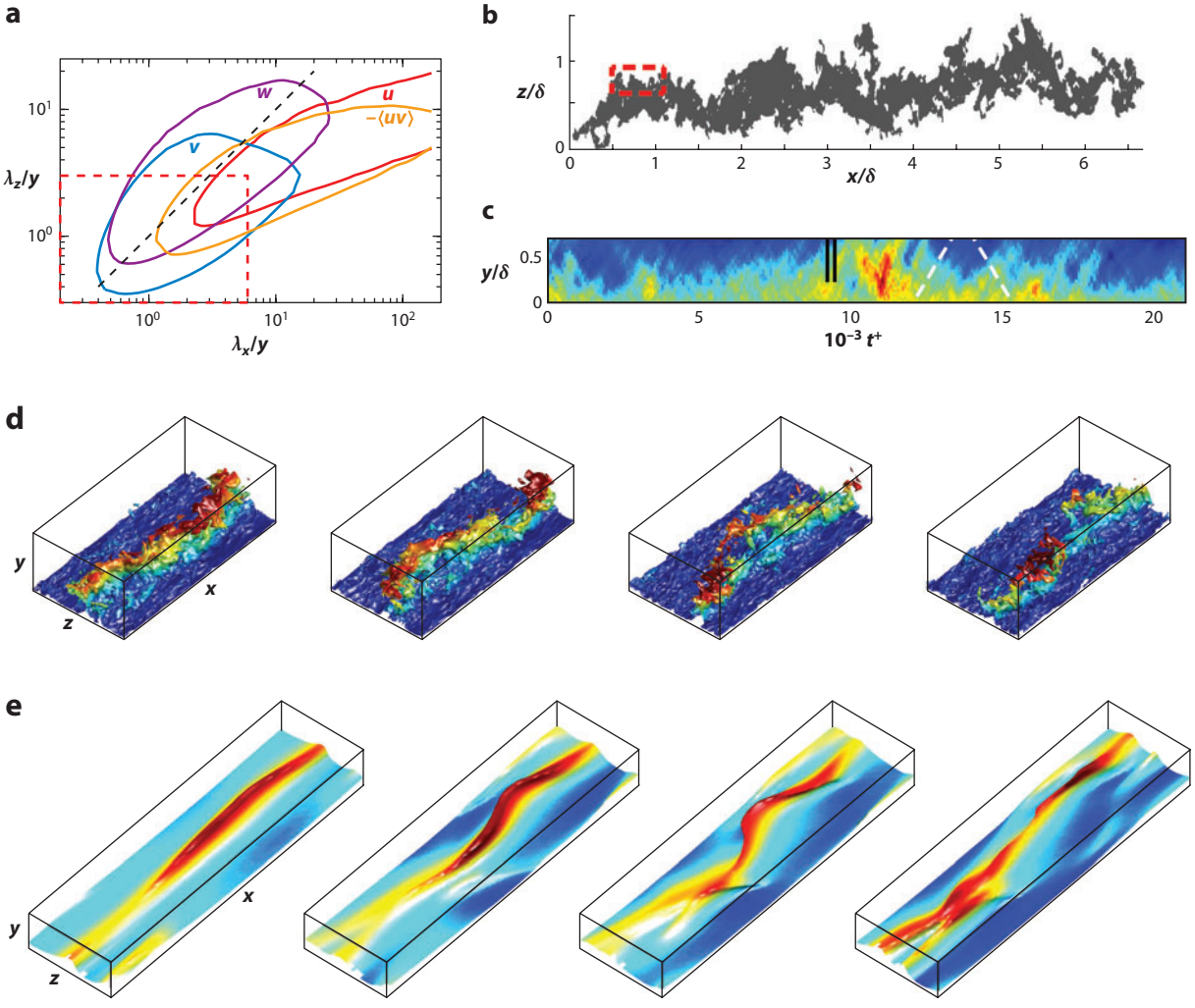

Figure 5

(*a*) Spectral densities of u (*red*), v (*blue*), w (*purple*), and $-\langle uv\rangle$ (*orange*) versus wavelengths scaled with the wall distance ($y/\delta = 0.15$). Isolines are 0.4 times the maximum of each spectrum, and the dashed diagonal line is $\lambda_x = \lambda_z$. (*b*) Long logarithmic-layer streak at $y^+ = 200$, defined as $u < -u'$. The tick marks in the x axis are 1,000 wall units apart. The dashed boxes in panels *a* and *b* are ($6y \times 3y$), and $\delta^+ = 2{,}000$. (*c*) Temporal evolution of $-\langle uv\rangle_{xz}$, averaged over wall-parallel planes of a small-box simulation, $L_x^+ \times \delta^+ \times L_z^+ = 2{,}900 \times 1{,}800 \times 1{,}450$. The white dashed lines are $\mathrm{d}y/\mathrm{d}t = \pm u_\tau$. (*d*) Time evolution of the $U^+ = 15$ isosurface during the burst marked by the two vertical lines in panel *c*. Colors are the distance from the wall, with red denoting $y = 0.4\delta$. Figure adapted from Flores & Jiménez (2010). (*e*) Isosurfaces of $U^+ = 8$, colored by the distance to the wall, with red denoting $y^+ = 30$. The flow in panels *d* and *e* is from bottom left to top right, and time marches toward the right. The axes move to keep the waves approximately steady.

Marusic (2007) and may refer to the same composite character, whereas Jiménez et al. (2004) showed that the very long streaks of the buffer layer, which pose a similar problem, are also formed from smaller components. The mechanism by which those subunits align themselves is unknown and remains one of the minor puzzles raised by wall-bounded flows, although del Álamo et al. (2006) noted that the lifetimes implied by the lengths of VLSMs are much longer than those

BURSTING

The meaning of bursting in wall-bounded turbulence has evolved over time. The original article by Kline et al. (1967) describes it as a time-dependent phenomenon associated with the sudden lifting of hydrogen bubbles from the wall, but later work tended to favor the interpretation that the temporal dependence is an artifact of the observation technique, caused by slowly changing structures, typically vortices, passing near the probe. The review by Robinson (1991), dealing mostly with simulation results, did much to solidify that view. However, the minimal simulations of Jiménez & Moin (1991) showed wide temporal variations of the intensities of individual turbulent structures, much closer to the original experimental description than to the later structural view. The results reviewed in the main text suggest that, although most of the fluctuations detected by stationary probes are almost surely due to passing sweeps and ejections, the intensity of those structures varies substantially when they are followed individually over time and that the violent events observed by Kline et al. (1967) were real, independent of the probe location.

measured for the clusters, suggesting that the latter could be consequences of the former, rather than the opposite.

An interesting recent finding is that the logarithmic layer can be simulated in relatively small numerical boxes, periodic in the two wall-parallel directions (Flores & Jiménez 2010), in roughly the same way as the buffer layer can be simulated in the minimal boxes described by Jiménez & Moin (1991). The two cases are not identical. When the logarithmic boxes are made smaller, turbulence does not decay, as it does in the buffer layer, but instead becomes restricted to a thinner region near the wall. In that sense, the minimal boxes of Jiménez & Moin (1991) are the innermost members of a hierarchy in which progressively smaller wall-attached structures are isolated by progressively smaller numerical boxes. The special feature of the buffer-layer minimal boxes is that they cannot be restricted any further.

The critical dimension is the spanwise periodicity, which limits turbulence to $y \lesssim 0.3L_z$. A box of the minimum dimensions suggested by those simulations, $L_x \times L_z = 6y \times 3y$, has been superimposed in **Figure 5*a*,*b*** and roughly agrees with the structures in **Figure 4**.

As in the case of the buffer layer, small-box simulations can be used to study the dynamics of the elementary stress-carrying structures of the logarithmic layer. Each box contains a single large-scale streamwise-velocity streak that bursts intermittently (see the sidebar Bursting). An example is given in **Figure 5*c***, which displays the evolution of the instantaneous Reynolds stress averaged over wall-parallel planes, $-\langle uv \rangle_{xz}$, as a function of wall distance and time. Both ascending and descending bursts can be seen, and Flores & Jiménez (2010) showed that they correspond to times when the ejection or the sweep predominates. It is interesting that their ascending and descending velocities are similar, $O(u_\tau)$, and remarkably uniform, suggesting that the two events are linked. Older qualitative descriptions of structures also mention that sweeps and ejections follow each other, but because they originate mostly from single-point observations, they were usually interpreted as describing the spatial organization of a structure being advected by the probe, whereas the above discussion refers to a true temporal evolution.

The evolution of the velocity field during the burst is shown in **Figure 5*d*** and looks remarkably similar to the bursting events described in the buffer layer by Jiménez & Moin (1991) and Jiménez et al. (2005), a sample of which is shown in **Figure 5*e***. In both cases, the single streak in the simulation box becomes increasingly wavy and is eventually destroyed by the burst, but the width of the boxes in **Figure 5*d*** is $L_z^+ = 1{,}500$, 15 times wider than those in **Figure 5*e***, and the streak in them is a fully turbulent multiscale object. The bursting period, T, can be estimated from the temporal evolution of different integrated quantities and depends on the distance to the wall as

$u_\tau T \approx 6y$, rather than on the size of the box. Wider boxes simply continue the linear trend further from the wall. We know less about the temporal evolution of the structures in unconstrained flows, but the temporal variability of the statistics of the minimal logarithmic boxes is essentially the same as the variability among randomly chosen sub-boxes of the same size in full channels, suggesting that the processes are similar in the full and minimal systems.

That turbulence can be simulated up to a given wall distance, with essentially correct statistics, even when the larger structures above it are not well represented, suggests that logarithmic-layer turbulence is independent from the core flow, in the same sense as the buffer layer is autonomous from the logarithmic region. It is also probably true that the logarithmic region is not controlled by the buffer layer, as shown by experiments in which the latter is disorganized without any clear effect on the former (Flores et al. 2007), and by the relative independence of the logarithmic layer from wall roughness, reviewed by Jiménez (2004) and more recently confirmed by Volino et al. (2007).

Taken together, those observations suggest that logarithmic-layer eddies of a given size are basically local to a single wall distance, although they have to cascade to smaller structures closer to the wall. However, in the same way that the buffer layer is modulated by the larger structures above it, we can expect some modulation of the logarithmic layer, including possibly long-range ordering, from the global modes above it.

6. DISCUSSION

Perhaps the most interesting conclusions that can be derived from the information obtained from new experiments and simulations are that the structure of the logarithmic layer appears to agree reasonably well with Townsend's (1961) classical model of a superposition of self-similar attached eddies and that the smaller scales are in rough equilibrium with the local velocity gradients created by the larger ones. The basic unit seems to be a family of eddies with aspect ratios $L_x \times L_y \times L_z \approx 5 \times 1 \times 2$, which, when they reach the boundary-layer thickness, $L_y = \delta$, agree with the LSMs observed in experiments. Each eddy, including its underlying energy and momentum cascades, can be isolated in a minimal unit, proportional to its height, within which its evolution seems to be essentially natural.

Above we describe two models for those structures: one as trains of hairpins and another as disorganized vortex clusters, associated on average with a side-by-side pair of a sweep and an ejection. As noted, the experimental support for the first type of arrangement is weak much above the buffer layer.

Kinematically, some of the differences between the two models are probably notational. For example, individual hairpins could correspond to the instabilities of the shear layers around the streaks created by the ejections, especially if hairpins were allowed to be irregular or incomplete, and the respective emphases on vortices and on larger eddies might be influenced by the relatively coarse resolution of many experiments, which cannot resolve individual vortices. Relying on conditional averages, such as in **Figure 4*a***, or on limited statistics based on selected recognizable objects, such as in **Figure 4*b***, might give an impression of symmetry that does not apply to more typical individual structures. Dynamically, it is harder to reconcile the respective treatments of the importance of the wall. The model implied by the minimal simulations and by roughness experiments emphasizes the effect of the local velocity shear, whereas the experimental model appears to require the formation of hairpins at, or near, the buffer region. That question cannot be fully resolved until we know more about the temporal evolution of those structures, but that will presumably change in the near future with the analysis of fully resolved flow animations (Lozano-Durán & Jiménez 2010).

Above we note that the individual eddies tend to align into much longer units and that the mechanism for the alignment remains unknown, but there are some indications that logarithmic-layer structures may be organized by larger eddies further from the wall.

SUMMARY POINTS

1. The logarithmic layer is the reflection of a multiscale momentum cascade.
2. The logarithmic cascade is carried by a self-similar Townsend hierarchy of wall-attached eddies.
3. Each attached eddy contains, on average, a sweep, an ejection, and an associated vortex cluster and includes a cascade of smaller attached eddies.
4. Attached eddies reach the wall as large-scale irrotational motions, but they are not controlled by buffer-layer processes.
5. Smaller scales are in approximate equilibrium with the local coarse-grained velocity gradient, both near and far from the wall.
6. Eddies in the buffer and logarithmic layers can be simulated and studied in minimal boxes, even if log-layer eddies are always turbulent objects.

FUTURE ISSUES

1. Numerical simulations with Reynolds numbers high enough to develop unambiguous theories of the inertial turbulent cascades, both isotropic and logarithmic, should be conducted within the next decade.
2. Simulations (and experiments) of the space- and time-resolved evolution of turbulent flows are needed within the next few years, which will allow testing of dynamical turbulence theories.
3. Linearized analysis is needed to clarify the energy-production mechanism of turbulent flow, but the details to be considered are still uncertain.
4. Perhaps the most intriguing open problem is how the fluctuation intensities adjust themselves among different wall distances to satisfy the momentum balance.

DISCLOSURE STATEMENT

The author is not aware of any biases that might be perceived as affecting the objectivity of this review.

ACKNOWLEDGMENTS

The preparation of this article has been supported in part by the Spanish CICYT, under grant TRA2009-11498, and by the European Research Council Advanced Grant ERC-2010-AdG-20100224. The author cordially thanks A. Lozano-Durán for assistance in creating **Figure 4**.

LITERATURE CITED

Abe H, Kawamura H, Matsuo Y. 2004. Surface heat-flux fluctuations in a turbulent channel flow up to $Re_\tau = 1020$ with $Pr = 0.025$ and 0.71. *Int. J. Heat Fluid Flow* 25:404–19

Clearly summarizes the hairpin-packet model for the lower logarithmic layer.

Adrian RJ. 2007. Hairpin vortex organization in wall turbulence. *Phys. Fluids* 19:041301

AGARD. 1998. A selection of test cases for the validation of large-eddy simulations of turbulent flows. *Advis. Rep. 345*, AGARD, Neuilly-sur-Seine, France; **http://torroja.dmt.upm.es/ftp/AGARD/docs/AGARD-AR-345.pdf**

Balakumar BJ, Adrian RJ. 2007. Large- and very-large-scale motions in channel and boundary-layer flow. *Philos. Trans. R. Soc. A* 365:665–81

Benzi R, Amati G, Casciola CM, Toschi F, Piva R. 1999. Intermittency and scaling laws for wall-bounded turbulence. *Phys. Fluids* 11:1284–86

Bertschy R, Chin RW, Abernathy FH. 1983. High-strain-rate free-surface boundary-layer flows. *J. Fluid Mech.* 126:443–61

Blackwelder RF, Kaplan RE. 1976. On the wall structure of the turbulent boundary layer. *J. Fluid Mech.* 76:89–112

Bogard DG, Tiederman WG. 1986. Burst detection with single-point velocity measurements. *J. Fluid Mech.* 162:389–413

Brown GL, Roshko A. 1974. On the density effects and large structure in turbulent mixing layers. *J. Fluid Mech.* 64:775–816

Butler KM, Farrell BF. 1993. Optimal perturbations and streak spacing in wall-bounded shear flow. *Phys. Fluids A* 5:774–77

Carlier J, Stanislas M. 2005. Experimental study of eddy structures in a turbulent boundary layer using particle image velocimetry. *J. Fluid Mech.* 535:143–88

Corrsin S. 1958. Local isotropy in turbulent shear flow. *NACA Res. Memo 58B11*, Washington, DC

Darcy H. 1854. Recherches expérimentales rélatives au mouvement de l'eau dans les tuyeaux. *Mém. Savants Etrang. Acad. Sci. Paris* 17:1–268

deGraaff DB, Eaton JK. 2000. Reynolds number scaling of the flat-plate turbulent boundary layer. *J. Fluid Mech.* 422:319–46

del Álamo JC, Jiménez J. 2003. Spectra of very large anisotropic scales in turbulent channels. *Phys. Fluids* 15:L41–44

del Álamo JC, Jiménez J. 2006. Linear energy amplification in turbulent channels. *J. Fluid Mech.* 559:205–13

del Álamo JC, Jiménez J. 2009. Estimation of turbulent convection velocities and corrections to Taylor's approximation. *J. Fluid Mech.* 640:5–26

Discusses the scaling and geometry of the energy spectra above the buffer layer.

del Álamo JC, Jiménez J, Zandonade P, Moser RD. 2004. Scaling of the energy spectra of turbulent channels. *J. Fluid Mech.* 500:135–44

del Álamo JC, Jiménez J, Zandonade P, Moser RD. 2006. Self-similar vortex clusters in the logarithmic region. *J. Fluid Mech.* 561:329–58

Flores O, Jiménez J. 2008. The structure of momentum transfer in turbulent channels. *Proc. Div. Fluid Dyn.*, PA-08. College Park, MD: Am. Phys. Soc.

Demonstrates that the attached-eddy cascade of the logarithmic layer can be simulated as a periodic array of minimal units.

Flores O, Jiménez J. 2010. Hierarchy of minimal flow units in the logarithmic layer. *Phys. Fluids* 22:071704

Flores O, Jiménez J, del Álamo JC. 2007. Vorticity organization in the outer layer of turbulent channels with disturbed walls. *J. Fluid Mech.* 591:145–54

Ganapathisubramani B, Longmire E, Marusic I. 2003. Characteristics of vortex packets in turbulent boundary layers. *J. Fluid Mech.* 478:35–46

Gaster M, Kit E, Wygnanski I. 1985. Large-scale structures in a forced turbulent mixing layer. *J. Fluid Mech.* 150:23–39

Guala M, Hommema SE, Adrian R. 2006. Large-scale and very-large-scale motions in turbulent pipe flow. *J. Fluid Mech.* 554:521–42

Hagen GHL. 1839. Über den Bewegung des Wassers in engen cylindrischen Röhren. *Poggendorfs Ann. Phys. Chem.* 46:423–42

Herpin S. 2010. *Study on the influence of the Reynolds number on the organization of wall-bounded turbulence*. PhD thesis. Mech. Eng., Ecole Cent. Lille

Hoyas S, Jiménez J. 2006. Scaling of the velocity fluctuations in turbulent channels up to $Re_\tau = 2003$. *Phys. Fluids* 18:011702

Hoyas S, Jiménez J. 2008. Reynolds number effects on the Reynolds-stress budgets in turbulent channels. *Phys. Fluids* 20:101511

Hultmark M, Vallikivi M, Smits AJ. 2010. Roughness effects on fully developed pipe flow at high Reynolds numbers. *Proc. Div. Fluid Dyn.*, GB-07. College Park, MD: Am. Phys. Soc.

Hutchins N, Marusic I. 2007. Evidence of very long meandering features in the logarithmic region of turbulent boundary layers. *J. Fluid Mech.* 579:467–77

Iwamoto K, Tsukahara T, Nakano H, Kawamura H. 2006. Effect of large-scale structures upon near-wall turbulence. *IUTAM Symp. Comput. Phys. New Perspect. Turbul.*, ed. Y Kaneda, pp. 53–58. New York: Springer

Jiménez J. 1998. The largest scales of turbulence. In *CTR Annu. Res. Briefs*, ed. P Moin, pp. 137–54. Stanford, CA: Stanford Univ.

Jiménez J. 2004. Turbulent flows over rough walls. *Annu. Rev. Fluid Mech.* 36:173–96

Jiménez J. 2007. Recent developments in wall-bounded turbulence. *Rev. R. Acad. Cienc. Ser. A* 101:187–203

Jiménez J. 2009. Inner-outer interactions in wall-bounded turbulence. In *Turbulence and Interactions*, ed. M Deville, TH Le, P Sagaut, pp. 3–14. New York: Springer

Jiménez J, del Álamo JC, Flores O. 2004. The large-scale dynamics of near-wall turbulence. *J. Fluid Mech.* 505:179–99

Jiménez J, Hoyas S. 2008. Turbulent fluctuations above the buffer layer of wall-bounded flows. *J. Fluid Mech.* 611:215–36

Jiménez J, Hoyas S, Simens MP, Mizuno Y. 2010. Turbulent boundary layers and channels at moderate Reynolds numbers. *J. Fluid Mech.* 657:335–60

Jiménez J, Kawahara G, Simens MP, Nagata M, Shiba M. 2005. Characterization of near-wall turbulence in terms of equilibrium and 'bursting' solutions. *Phys. Fluids* 17:015105

Jiménez J, Moin P. 1991. The minimal flow unit in near-wall turbulence. *J. Fluid Mech.* 225:221–40

Jiménez J, Pinelli A. 1999. The autonomous cycle of near wall turbulence. *J. Fluid Mech.* 389:335–59

Jiménez J, Wray AA, Saffman PG, Rogallo RS. 1993. The structure of intense vorticity in isotropic turbulence. *J. Fluid Mech.* 255:65–90

Kawahara G, Uhlmann M, van Veen L. 2012. The significance of simple invariant solutions in turbulent flows. *Annu. Rev. Fluid Mech.* 44:203–25

Kim HT, Kline SJ, Reynolds WC. 1971. The production of turbulence near a smooth wall in a turbulent boundary layer. *J. Fluid Mech.* 50:133–60

Kim J, Moin P, Moser RD. 1987. Turbulence statistics in fully developed channel flow at low Reynolds number. *J. Fluid Mech.* 177:133–66

Kim K, Adrian RJ. 1999. Very large-scale motion in the outer layer. *Phys. Fluids* 11:417–22

Klewicki JC, Metzger MM, Kelner E, Thurlow E. 1995. Viscous sublayer flow visualizations at $R_\theta \approx 1{,}500{,}000$. *Phys. Fluids* 7:857–63

Kline SJ, Reynolds WC, Schraub FA, Runstadler PW. 1967. Structure of turbulent boundary layers. *J. Fluid Mech.* 30:741–73

Kolmogorov AN. 1941. The local structure of turbulence in incompressible viscous fluids for very large Reynolds numbers. *Dokl. Akad. Nauk. SSSR* 30:301–5

Kolmogorov AN. 1962. A refinement of previous hypotheses concerning the local structure of turbulence in a viscous incompressible fluid at high Reynolds number. *J. Fluid Mech.* 13:82–85

Kunkel GJ, Marusic I. 2006. Study of the near-wall-turbulent region of the high-Reynolds-number boundary layer using atmospheric data. *J. Fluid Mech.* 548:375–402

Lee SH, Sung HJ. 2007. Direct numerical simulation of the turbulent boundary layer over a rod-roughened wall. *J. Fluid Mech.* 584:125–46

Lee SH, Sung HJ. 2011. Direct numerical simulation of a turbulent boundary layer up to $Re_\theta = 2500$. *Int. J. Heat Fluid Flow* 32:1–10

Lozano-Durán A, Jiménez J. 2010. Time-resolved evolution of the wall-bounded vorticity cascade. *Proc. Div. Fluid Dyn.*, EB-3. College Park, MD: Am. Phys. Soc.

Marusic I, Mathis R, Hutchins N. 2010. Predictive model for wall-bounded turbulent flow. *Science* 329:193–96

Characterizes near-wall turbulence as an autonomous cycle of streaks and vortices.

Presents the first experimental characterization of the life cycle of sublayer streaks.

Presents the first and seminal direct simulation of a turbulent wall-bounded flow.

Demonstrates that the sublayer streaks persist with few changes up to atmospheric Reynolds numbers.

Mathis R, Hutchins N, Marusic I. 2009. Large-scale amplitude modulation of the small-scale structures in turbulent boundary layers. *J. Fluid Mech.* 628:311–37

Summarizes the state of wall-turbulence research up to 2006.

McKeon BJ. 2007. Scaling and structure in high Reynolds number wall-bounded flows. *Philos. Trans. R. Soc. A* 365:633–876

Meinhart CD, Adrian RJ. 1995. On the existence of uniform momentum zones in a turbulent boundary layer. *Phys. Fluids* 7:694–96

Metzger MM, Klewicki JC. 2001. A comparative study of near-wall turbulence in high and low Reynolds number boundary layers. *Phys. Fluids* 13:692–701

Metzger MM, Klewicki JC, Bradshaw K, Sadr R. 2001. Scaling of near-wall axial turbulent stress in the zero pressure gradient boundary layer. *Phys. Fluids* 13:1819–21

Millikan CB. 1938. A critical discussion of turbulent flows in channels and circular tubes. *Proc. 5th Int. Conf. Appl. Mech.*, pp. 386–92. New York: Wiley

Monty JP, Hutchins N, Ng HCH, Marusic I, Chong MS. 2009. A comparison of turbulent pipe, channel and boundary layer flows. *J. Fluid Mech.* 632:431–42

Obukhov AM. 1941. On the distribution of energy in the spectrum of turbulent flow. *Dokl. Akad. Nauk. SSSR* 32:22–24

Österlund JM, Johansson AV, Nagib HM, Hites M. 2000. A note on the overlap region in turbulent boundary layers. *Phys. Fluids* 12:1–4

Panton RL. 2001. Overview of the self-sustaining mechanisms of wall turbulence. *Prog. Aerosp. Sci.* 37:341–85

Presents the eddy-forest model of the logarithmic layer and first clear evidence for the k^{-1} spectrum.

Perry AE, Henbest SM, Chong MS. 1986. A theoretical and experimental study of wall turbulence. *J. Fluid Mech.* 165:163–99

Perry AE, Li JD. 1990. Experimental support for the attached-eddy hypothesis in zero-pressure-gradient turbulent boundary layers. *J. Fluid Mech.* 218:405–38

Reynolds WC, Tiederman WG. 1967. Stability of turbulent channel flow, with application to Malkus' theory. *J. Fluid Mech.* 27:253–72

Richardson LF. 1920. The supply of energy from and to atmospheric eddies. *Proc. R. Soc. A* 97:354–73

Robinson SK. 1991. Coherent motions in the turbulent boundary layer. *Annu. Rev. Fluid Mech.* 23:601–39

Saddoughi SG, Veeravali SV. 1994. Local isotropy in turbulent boundary layers at high Reynolds numbers. *J. Fluid Mech.* 268:333–72

Schlatter P, Örlü R, Li Q, Fransson J, Johansson A, et al. 2009. Turbulent boundary layers up to $Re_\theta = 2500$ through simulation and experiments. *Phys. Fluids* 21:051702

Schmid PJ. 2007. Nonmodal stability theory. *Annu. Rev. Fluid Mech.* 39:129–62

Schoppa W, Hussain F. 2002. Coherent structure generation in near-wall turbulence. *J. Fluid Mech.* 453:57–108

Sillero JA, Borrell G, Gungor AG, Jiménez J, Moser R, Oliver TA. 2010. Direct simulation of the zero-pressure-gradient boundary layer up to $Re_\theta = 6000$. *Proc. Div. Fluid Dyn.*, EB-4. College Park, MD: Am. Phys. Soc.

Simens M, Jiménez J, Hoyas S, Mizuno Y. 2009. A high-resolution code for turbulent boundary layers. *J. Comput. Phys.* 228:4218–31

Smits AJ, MacKeon BJ, Marusic I. 2011. High–Reynolds number wall turbulence. *Annu. Rev. Fluid Mech.* 43:353–75

Tanahashi M, Kang SJ, Miyamoto T, Shiokawa S, Miyauchi T. 2004. Scaling law of fine scale eddies in turbulent channel flows up to $Re_\tau = 800$. *Int. J. Heat Fluid Flow* 25:331–40

Tennekes H, Lumley JL. 1972. *A First Course in Turbulence*. Cambridge, MA: MIT Press

Tomkins CD, Adrian RJ. 2003. Spanwise structure and scale growth in turbulent boundary layers. *J. Fluid Mech.* 490:37–74

Presents the original attached-eddy model of the logarithmic layer.

Townsend AA. 1961. Equilibrium layers and wall turbulence. *J. Fluid Mech.* 11:97–120

Townsend AA. 1976. *The Structure of Turbulent Shear Flow*. Cambridge, UK: Cambridge Univ. Press. 2nd ed.

Volino RJ, Schultz MP, Flack KA. 2007. Turbulence structure in rough- and smooth-wall boundary layers. *J. Fluid Mech.* 592:263–93

Wallace JM, Eckelmann H, Brodkey RS. 1972. The wall region in turbulent shear flow. *J. Fluid Mech.* 64:39–48

Wark CE, Nagib HM. 1991. Experimental investigation of coherent structures in turbulent boundary layers. *J. Fluid Mech.* 230:183–208

Willmarth WW, Lu S. 1972. Structure of Reynolds stress near wall. *J. Fluid Mech.* 55:65–92

Wu X, Moin P. 2010. Transitional and turbulent boundary layer with heat transfer. *Phys. Fluids* 22:085105

Wu Y, Christensen KT. 2005. Population trends of spanwise vortices in wall turbulence. *J. Fluid Mech.* 568:55–76